MULTI-OBJECTIVE BAYESIAN OPTIMIZATION OF MULTI-STAGE OK-SASE FOR EFFICIENT HARD X-RAY FEL OPERATION

X. Liu[1,2], H. Yang[2], N. Huang[2], J. Cai[1], H. Wen[1], J. Yu[*1], H. Deng[†2]
[1]Hunan University, School of Physics and Electronics, Hunan University, Changsha, China
[2]Shanghai Advanced Research Institute, Chinese Academy of Sciences, Shanghai, China

Abstract

High-photon-energy hard X-ray free-electron laser radiation enables unprecedented opportunities for probing matter at atomic scales, however, its generation remains challenging for self-amplified spontaneous emission (SASE)-based XFELs due to reduced FEL gain, leading to extended undulator requirements and limited radiation efficiency. To address this issue, we investigate a multi-stage optical-klystron SASE (OK-SASE) scheme that enhances microbunching through dispersive sections and shortens the gain length. A multi-objective Bayesian optimization (MOBO) framework is introduced to systematically optimize the configuration. Using SHINE as a representative case, steady-state simulations at 15 keV show that the optimized setup reduces the required undulator length relative to conventional SASE by about 7% to 22%, depending on the electron-beam energy spread. The optimization indicates that several chicanes can remain effectively inactive, enabling a more compact beamline layout. The time-dependent simulations also demonstrate the feasibility of multi-stage OK-SASE for efficient high-energy XFEL operation.

INTRODUCTION

The generation of hard X-ray free-electron laser pulses at very high photon energies is highly desirable for probing matter with atomic-scale spatial and temporal resolution [1]. However, as XFEL operation is extended toward higher photon energies, the FEL gain decreases significantly, leading to substantially increased saturation lengths in the self-amplified spontaneous emission (SASE) mode and posing significant challenges for the design of compact hard X-ray beamlines. This issue is particularly relevant to high-energy XFEL beamlines, such as FEL-III of SHINE, which covers the photon-energy range of 10-25 keV using superconducting undulators [2]. Multi-stage optical-klystron [3–5] (OK) configurations can enhance the FEL gain and shorten the saturation length, but their performance depends on the coordinated tuning of multiple dispersive sections. In this work, we combine the multi-stage OK-SASE scheme with multi-objective Bayesian optimization (MOBO) framework to optimize FEL configurations, using FEL-III as a representative case study. Chicane delays are optimized with saturation length and output performance as two objectives, and a shorter saturation length is preferred when selecting the representative solution. Optimization also reveals an efficient distribution of dispersive chicanes, indicating that several chicanes can remain inactive, enabling a more compact FEL configuration. Both steady-state and time-dependent simulations confirm the effectiveness of the proposed optimized scheme.

* jinqing.yu@hnu.edu.cn
† denghx@sari.ac.cn

METHODS

As shown in Fig. 1, the multi-stage OK-SASE layout consists of a series of undulators, with one dispersive chicane inserted between every two neighboring undulators. In this configuration, the energy modulation generated in an upstream undulator is converted by the following chicane into density modulation before the electron beam enters the next undulator. As a result, the microbunching is strengthened from stage to stage, leading to enhanced FEL gain. According to the one-dimensional theory of OK [3], the maximum gain is obtained when $2\pi R_{56}\sigma_\delta/\lambda_r \sim 1$, where λ_r is the radiation wavelength, R_{56} is the momentum compaction of the dispersive chicane, and σ_δ is the rms relative energy spread of the electron beam. The optical-klystron effect becomes more pronounced when $\sigma_\delta \ll \rho$, where ρ is the FEL Pierce parameter.

Based on the proposed layout described above, Bayesian optimization (BO) is employed to determine the operating configuration, as illustrated in Fig. 2. The chicane delays in the FEL-III beamline are taken as the optimization variables, denoted by $\mathbf{x} = (d_1, d_2, \ldots, d_N)$, where d_i is the delay of the ith chicane. Each delay is bounded within $d_i \in [0, d_i^{\max}]$, where the upper bound $d_i^{\max}$ is determined from the OK condition, while the lower bound is set to zero so that a given chicane can remain inactive. These variables define an N-dimensional search space for BO. The optimization is formulated as a bi-objective problem,

$$\mathbf{y}(\mathbf{x}) = \left(-z_{\mathrm{sat}}(\mathbf{x}),\, Q_{\mathrm{sat}}(\mathbf{x})\right),$$

where z_{sat} is the saturation length and Q_{sat} denotes the FEL output at saturation. The saturation length is defined using the accumulated beamline length, including the physical lengths of both undulators and chicanes, regardless of whether the chicane delay is zero. In the steady-state simulations, $Q_{\mathrm{sat}} = P_{\mathrm{sat}}$, while in the time-dependent simulations, $Q_{\mathrm{sat}} = E_{\mathrm{sat}}$, with $E(z) = \int P(t,z)\,dt$, where $P(t,z)$ is the temporal power profile at the longitudinal position z. The minus sign converts the minimization of z_{sat} into a maximization form. Each BO trial starts from an initial set of valid training samples. When no predefined initial dataset is available, the initial points are generated by Sobol sampling to provide a more uniform coverage of the search space.

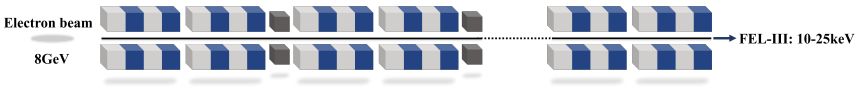

Figure 1: Schematic of the multi-stage OK-SASE layout for FEL-III. The dashed lines indicate that several repeated undulator–chicane stages are omitted for clarity.

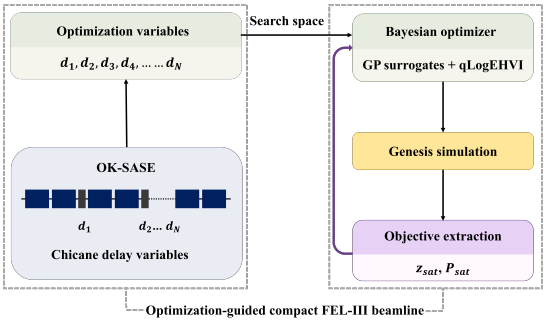

Figure 2: Schematic workflow of the bi-objective BO for the multi-stage OK-SASE configuration.

Based on these samples, separate Gaussian-process surrogate models are trained for the two objectives [6], and new candidate points are selected through the qLogEHVI acquisition function [7,8]. The reference point is defined from the SASE baseline as $\mathbf{r} = (-z_{\mathrm{sat}}^{\mathrm{SASE}} - \Delta z,\ Q_{\mathrm{sat}}^{\mathrm{SASE}} - \Delta Q)$, where Δz and ΔQ are small offsets introduced in the two objective directions. Since qLogEHVI is used in a batch setting, multiple candidate points can be proposed and evaluated in parallel at each iteration. For each candidate setting $\mathbf{x}$, a Genesis simulation [9] is performed. The saturation point is determined from the corresponding growth curve $G(z)$, where $G(z) = P(z)$ for the steady-state simulations and $G(z) = E(z)$ for the time-dependent simulations. The logarithmic gain is defined as $g(z) = \frac{d \log G(z)}{dz}$, and the threshold is taken as $g_{\mathrm{th}} = 0.1\, g_{\mathrm{max}}$, where g_{max} is the maximum logarithmic gain evaluated over the downstream 80% of the undulator. The first position at which $g(z)$ falls below g_{th} is identified as z_{sat}, and the corresponding output $G(z_{\mathrm{sat}})$ is taken as Q_{sat}. The newly evaluated results are then appended to the training data to update the surrogate models, and the optimization proceeds iteratively. The resulting trade-off solutions are characterized by the Pareto front.

SIMULATION RESULTS

In this section, we present the steady-state optimization results for the multi-stage OK-SASE configuration of FEL-III at 15 keV. The main electron beam and undulator parameters are listed in Table 1. In the present layout, adjacent undulator segments are separated by 0.5 m, and this spacing increases to 1.5 m when a chicane is inserted. As a baseline, the standard SASE configuration yields a saturation length of $z_{\mathrm{sat}}^{\mathrm{SASE}} = 118.57$ m and a saturation power of $P_{\mathrm{sat}}^{\mathrm{SASE}} = 1.87$ GW, which are taken as reference for comparison with the optimized configurations.

BO is then performed for the 16 chicane delays in the multi-stage OK-SASE layout, defining a 16-dimensional search space. The delay range is determined from the OK condition, and the upper bound is set to 6.6×10^{-8} m. To improve robustness, the optimization is repeated in five independent trials, each initialized with 12 valid samples and followed by 120 BO iterations with a batch size of $q = 2$, giving 600 newly evaluated candidate points in total. The Pareto front in Fig. 3(a) shows a clear trade-off between saturation length and saturation power. Shorter saturation lengths generally come with some loss of saturation power, while higher-power solutions tend to saturate later. A representative OK-SASE solution is selected from this front and compared with SASE in Fig. 3(b). The saturation point is shifted upstream from 118.57 m to 110.58 m, corresponding to a 6.7% reduction in the required undulator length, i.e. two undulators in the present layout. The saturation power decreases only from 1.87 GW to 1.78 GW, or by about 4.8%, showing that improved compactness can be achieved with only a limited performance penalty.

Table 1: Main Electron Beam and Undulator Parameters of FEL-III

Parameter	Value	Unit
Electron Beam		
Energy	8	GeV
Bunch charge	100	pC
Peak current	1500	A
Slice energy spread	0.01	%
Normalized emittance	0.45	mm·mrad
Undulator Line		
Period length	16.5	mm
Undulator length	3	m
Segment gap	0.5	m

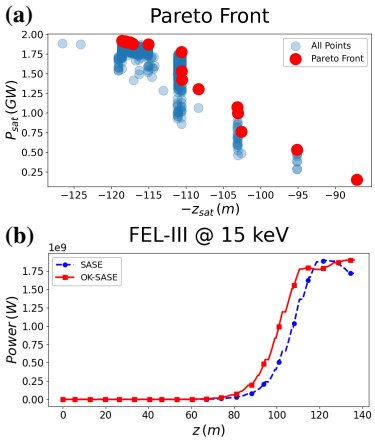

Figure 3: (a) Pareto front obtained from all evaluated solutions. (b) Comparison of the power evolution along the undulator between the selected OK-SASE solution and the SASE baseline at 15 keV.

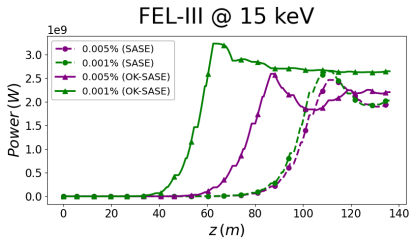

Figure 4: Comparison of the power evolution for optimized OK-SASE and SASE configurations at 15 keV for electron beam energy spreads of 0.005% and 0.001%.

The selected solution shows a sparse and non-uniform delay distribution. Several chicanes remain effectively inactive, while only a few require relatively large delays. This indicates that the performance improvement does not require all dispersive sections to be activated, which favors a simpler FEL-III chicane configuration.

The same optimization procedure is applied to cases with different electron beam energy spreads. As shown in Fig. 4, the optimized OK-SASE configurations shift the power-growth curve upstream relative to conventional SASE. For an energy spread of 0.005%, the saturation length is reduced from 110.57 m to 86.57 m, while the saturation power increases from 2.50 GW to 2.60 GW. For 0.001%, the improvement is more pronounced, with the saturation length reduced from 107.58 m to 62.55 m and the saturation power increased from 2.55 GW to 3.24 GW. These results show that a smaller energy spread markedly enhances the effectiveness of the optimized multi-stage OK-SASE scheme and suggests a favorable direction for the beam-parameter setting of FEL-III.

To assess the optimized scheme, the time-dependent simulations are also performed for the case with an electron beam energy spread of 0.005%. The optimization is carried out for the 16 chicane delays with five independent trials, 120 BO iterations in each trial, and a batch size of $q = 1$, using the pulse energy $E(z)$ as the growth curve. As shown in Fig. 5, a representative MOBO-optimized OK-SASE shifts the pulse-energy growth curve upstream and gives a higher peak power than SASE. Furthermore, the multi-shot behavior of the MOBO-optimized setup is evaluated against conventional SASE under shot-to-shot fluctuations. The averaged saturation lengths and pulse energies of 50 independent shots are 104.22 ± 2.65 m and 55.47 ± 4.78 μJ for SASE, and 95.00±0.13 m and 73.40±2.10 μJ for OK-SASE, respectively. The relative fluctuation of the saturation pulse energy, defined as the standard deviation divided by the mean value, is 8.61% for SASE and 2.87% for OK-SASE. The average saturation pulse energy obtained with the optimized OK-SASE setup is 32% higher than that of SASE, which is well above the intrinsic shot-to-shot fluctuation level. These multi-shot results indicate that, with the aid of MOBO, an effective chicane configuration can be identified for multi-stage OK-SASE operation, leading to a clear enhancement of the pulse energy in time-dependent simulations. This supports the effectiveness of the proposed optimization strategy for searching favorable OK-SASE setups for efficient XFEL operation.

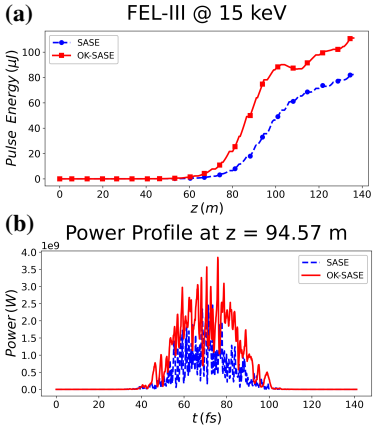

Figure 5: The representative time-dependent optimization results for FEL-III. (a) Pulse-energy evolution along the undulator for the optimized OK-SASE and SASE configurations. (b) Temporal power profiles of the two configurations.

CONCLUSION

This work develops an optimization method that combines multi-stage OK-SASE scheme with multi-objective Bayesian optimization framework to reduce the required undulator length while preserving competitive FEL performance. Using FEL-III as a representative case, the optimized OK-SASE configuration at 15 keV reduces the required undulator length by about 7%–22% relative to SASE, depending on the electron beam energy spread. The optimized chicane-delay distributions show that near-optimal performance can be achieved with only a subset of chicanes, providing practical guidance for a more compact FEL-III beamline configuration. In addition, a smaller electron beam energy spread further strengthens the OK effect and improves the optimization performance. Representative time-dependent simulations further show that the optimized OK-SASE scheme remains advantageous. In the present study, only chicane delays are included as optimization variables. Future work will consider more complex FEL configurations by incorporating additional variables, such as taper profiles and quadrupole settings, together with time-dependent start-to-end simulations.

ACKNOWLEDGMENTS

We extend our gratitude to Zheng Qi, Chenzhi Xu, and Bingyang Yan for their insightful discussions and keen interest in this work. This work was supported by the National Natural Science Foundation of China (Grant Nos. 12125508, 12541503, 12175058), National Science Fund of Hunan Province for Distinguished Young Scholars No. 2024JJ2009, the National Key Research and Development Program of China (2024YFA1612104), Shanghai Pilot Program for Basic Research – Chinese Academy of Sciences, Shanghai Branch (JCYJ-SHFY-2021-010), and China Postdoctoral Science Foundation (2025M770914).

REFERENCES

[1] N. Huang, *et al.*, "Features and futures of X-ray free-electron lasers", *The Innovation*, vol. 2, no. 2, p. 100097, 2021. doi:10.1016/j.xinn.2021.100097

[2] T. Liu, *et al.*, "Status and future of the soft X-ray free-electron laser beamline at the SHINE", *Front. Phys.*, vol. 11, p. 1172368, 2023. doi:10.3389/fphy.2023.1172368

[3] Y. Ding, *et al.*, "Optical klystron enhancement to self-amplified spontaneous emission free electron lasers", *Phys. Rev. Accel. Beams*, vol. 9, no. 7, p. 070702, 2006. doi:10.1103/PhysRevSTAB.9.070702

[4] E. Prat, *et al.*, "Demonstration of a compact x-ray free-electron laser using the optical klystron effect", *Appl. Phys. Lett.*, vol. 119, no. 15, p. 151102, 2021. doi:10.1063/5.0064934

[5] X. Liu *et al.*, "Multicolor x-ray free-electron laser generation using optical klystron for multiframe diffraction imaging", *Phys. Rev. Accel. Beams*, accepted, 2026. doi:10.1103/ygrv-6x6n

[6] C. E. Rasmussen and C. K. I. Williams, *Gaussian Processes for Machine Learning*, Cambridge, MA, USA: MIT Press, 2006, ISBN 9780262182539.

[7] S. Daulton, M. Balandat and E. Bakshy, "Differentiable Expected Hypervolume Improvement for Parallel Multi-Objective Bayesian Optimization", in *Adv. Neural Inf. Process. Syst.*, vol. 33, pp. 9851–9864, 2020. doi:10.48550/arXiv.2006.05078

[8] S. Ament, *et al.*, "Unexpected Improvements to Expected Improvement for Bayesian Optimization", in *Adv. Neural Inf. Process. Syst.*, vol. 36, pp. 20577–20612, 2023. doi:10.48550/arXiv.2310.20708

[9] S. Reiche, "GENESIS 1.3: a fully 3D time-dependent FEL simulation code", *Nucl. Instrum. Methods Phys. Res. A*, vol. 429, no. 1, pp. 243–248, 1999. doi:10.1016/S0168-9002(99)00114-X